# Loosely-Displaced Geostationary Orbits with Hybrid Sail Propulsion

**Yuan Liu [a*], Jeannette Heiligers [b], Matteo Ceriotti [c]**

[a] *College of Automation, Harbin Engineering University, Harbin 150001, China*

[b] *Faculty of Aerospace Engineering, Delft University of Technology, Delft, The Netherlands*

[c] *School of Engineering, University of Glasgow, Glasgow, United Kingdom*

## Abstract

To overcome the congestion of geostationary orbit slots, previous work proposed to use vertically-displaced, non-Keplerian geostationary orbits by means of continuous low-thrust propulsion in the form of hybrid solar sail and solar electric propulsion (hybrid sail). This work extends and generalizes that concept by loosening the position constraint and introducing a station-keeping box. Sub-optimal orbits are first found with an inverse method that still satisfy the geostationary position constraint (i.e., no station-keeping box), which will be referred to as ideal displaced geostationary orbits. For these sub-optimal orbits, it is found that the hybrid sail saves propellant mass compared to the pure solar electric propulsion case: for solar sail lightness numbers of up to a value of 0.2 and the most favorable time during the year (i.e., at summer solstice), the hybrid sail saves up to 71.6% propellant mass during a single day compared to the use of pure solar electric propulsion. Subsequently, the sub-optimal orbits are used as a first-guess for a direct optimization algorithm based on Gauss pseudospectral transcription, which loosens the position constraint. This enables a more flexible trajectory around the ideal displaced geostationary orbit and lets the solar sail contribute more efficiently to the required acceleration. It therefore leads to a further propellant savings of up to 73.8%. Finally, the mass budget shows that by using by using far-term solar sail technology, the hybrid propulsion system enables an evident reduction in the required initial mass of the spacecraft for a given payload mass with a relatively long mission duration.

**Keywords:** displaced geostationary orbits; orbit optimization; hybrid propulsion; solar sail

*Corresponding author. Tel.: +86 13633660098

*E-mail address: ericliuprc@hotmail.com*

## I. Introduction[1]

The geostationary orbit (GEO) is a circular, equatorial orbit whose period equals the Earth's rotational period and its orbital radius therefore equals approximately 42,164 km. It allows a satellite to be stationary above a certain point on the Earth's equator. With the advantage of being stationary, GEO satellites are largely used for telecommunications and Earth observation (mainly meteorology). The GEO is a unique and currently very congested orbit, especially at longitudes above densely populated areas [1].

Highly non-Keplerian orbits (NKOs) are trajectories that can be achieved by a continuous control acceleration generated by the spacecraft, which was systematically introduced by Mckay et al. [2]. By partially offsetting or complementing the effects of gravity, NKOs show evident advantages in that new orbits can be designed. The design [4-10], optimization [4-10], stability and control [11-13] of NKOs have been researched extensively; proposed applications range from pole-sitters [3,4], lunar far-side communication and lunar south-pole coverage [5-7], Mars, Mercury and Venus remote sensing [7,8], further Mars exploration [9], to near-Earth asteroids rendezvous [10]. The concept of using an NKO to displace the GEO has already been proposed [1] and the existence of light-levitated GEOs for solar sailing has already been shown by Baig and McInnes [14]. This paper studies the optimal design of loosely-displaced GEOs and proposes the use of solar sail propulsion and solar electric propulsion (SEP) on the same spacecraft (hybrid sail propulsion).

Although solar sailing is a relatively old notion, it has many high-demanding technology requirements on materials, control and structures [15]. Only recently, three small sail demonstrator missions were deployed: one by JAXA, the Interplanetary Kite-Craft Accelerated by Radiation of the Sun (IKAROS); one by NASA, NanoSail-D2; and one by The Planetary Society, LightSail-1 [16-18]. In addition, the NEA Scout mission plans to launch a CubeSat-sized spacecraft propelled by a solar sail for near-Earth asteroid exploration mid-2018 [19]. Much research has focused on using solar sailing as the primary propulsion system on a spacecraft to maintain NKOs [20-23]. However, there are still some challenges to overcome, such as the difficulties of designing and building large and lightweight membrane structures. In addition, the solar sail is unable to generate a thrust component towards the Sun [15]. Compared to solar sailing, SEP relies on a finite onboard propellant source, but is a much more mature and near-term technology. It can produce a relatively low thrust with high specific impulse. It has been successfully used in several space missions, including Deep Space 1 (1998) [24], the Gravity Field and Steady-State Ocean Circulation Explorer (GOCE, 2009) [25], and

SMART-1 [26].

Considering the complementarity of solar sailing and SEP, the concept of hybridizing a relatively small, near-term solar sail and SEP has been previously proposed [3, 27]. In this field, research is flourishing, aiming to maximize the potential of the hybrid sail propulsion system. Proposed concepts include optimal transfers from Earth to Venus and Mars [28, 29], optimal trajectories for Earth pole-sitters [3, 4], pole-sitters at other planets [8], and displaced orbits in the Earth-Moon system [30]. As those studies show, the hybrid sail has better performance in terms of long-term propellant consumption than pure SEP and lower technological challenge than a large solar sail, at the cost of increased system and control complexity.

In this work, a generalization of the hybrid-sail displaced geostationary orbit (DGEO) proposed by Heiligers et al. [1] is presented and discussed. We relax the constraint of a constant relative position with respect to an Earth observer, while keeping the spacecraft in an assigned station-keeping box, generating a loosely-displaced GEO (LDGEO). It is expected that, by releasing the constraint on the position, additional propellant can be saved by the hybrid sail/SEP combination. We indeed show that propellant can be saved, because the station-keeping box allows the orbit to be tilted which allows the solar sail to operate more efficiently and therefore reduces the total SEP thrust required. However, the introduction of the concept of a station-keeping box comes with the drawback that the spacecraft is not perfectly stationary above a point on the Earth, and thus not truly "geostationary". This could cause potential pointing problems. However, we show that, if the station-keeping box is small enough, the effects of pointing problems can be restricted to an acceptable level such that this displacement will not be perceivable from Earth.

The remainder of the paper is organized as follows: after a brief description of the hybrid sail dynamics (Sec. II), Sec. III explains the concept of the DGEO. It then presents an inverse method to minimize the SEP thrust and obtain the corresponding solar sail control for an ideal DGEO, i.e., without a station-keeping box. Those results are subsequently used as a first-guess for a Gauss-pseudospectral algorithm that does include a station-keeping box, which solves the optimal control problem numerically. Finally, Sec. IV discusses the optimal mass budget for a hybrid sail spacecraft for different sail sizes and mission lifetimes.

## II. Equations of Motion

The ideal DGEO is an NKO which is parallel to the equatorial plane (above or below) and whose period equals the Earth's rotational period. Compared to the distance from the Sun, a spacecraft in a DGEO is much closer to the Earth. Therefore, the dynamics are defined as two-body, Earth-centered dynamics, neglecting perturbations from the higher

order harmonics from the Earth's potential, the Moon, Sun, and so on. A rotating reference frame, $A(X,Y,Z)$ is considered in which the origin is at the center of the Earth; the $X$ axis points towards the ideal DGEO satellite's projection on the equatorial plane; the $Z$ axis is aligned with the angular momentum vector of the Earth and perpendicular to the equatorial plane, and the $Y$ axis completes the right-handed Cartesian reference frame (see Fig. 1). In the following, all vectors are expressed in this frame unless specified by a different superscript. The equations that describe the motion of the spacecraft in the rotating reference frame are

$$\begin{cases} \ddot{x} = 2\omega_e \dot{y} + \omega_e{}^2 x - \dfrac{\mu_e x}{r^3} + a_X \\ \ddot{y} = -2\omega_e \dot{x} + \omega_e{}^2 y - \dfrac{\mu_e y}{r^3} + a_Y \\ \ddot{z} = -\dfrac{\mu_e z}{r^3} + a_Z \end{cases} \tag{1}$$

Considering the $X$, $Y$ and $Z$ axes, the spacecraft position vector is $\mathbf{r}=[x, y, z]^{\mathrm{T}}$, $r=\|\mathbf{r}\|$, $\omega_e$ is the Earth's constant angular velocity and $\mu_e$ is the gravitational parameter of the Earth. Furthermore, a thrust-induced acceleration $\mathbf{a}=[a_X, a_Y, a_Z]^{\mathrm{T}}$ is assumed to maintain the DGEO. For a hybrid sail propulsion system, $\mathbf{a}$ consists of two parts, which can be written as

$$\mathbf{a} = \mathbf{a}_{\mathrm{S}} + \mathbf{a}_{\mathrm{SEP}} \tag{2}$$

where $\mathbf{a}_{\mathrm{S}}$ is the contribution of the solar sail and $\mathbf{a}_{\mathrm{SEP}}$ is the contribution of the SEP thruster.

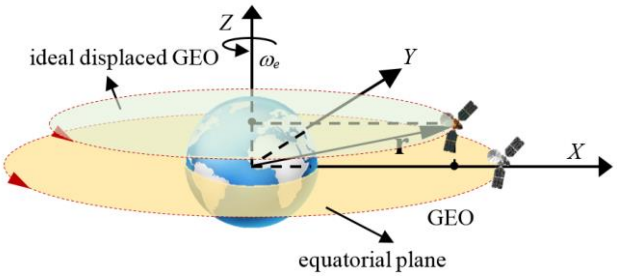


Fig. 1 DGEO in the rotating reference frame ($A$)

Because frame ($A$) rotates at the same angular speed as the Earth's rotation, the DGEO is represented by a stationary point. Therefore, the spacecraft's position with respect to the $Y$ axis, the velocity $\dot{\mathbf{r}}=[\dot{x}, \dot{y}, \dot{z}]^{\mathrm{T}}$ and the acceleration $\ddot{\mathbf{r}}=[\ddot{x}, \ddot{y}, \ddot{z}]^{\mathrm{T}}$ are all equal to 0. Then, the equilibrium solutions can be obtained by eliminating the motion-related terms from Eq. (1):

$$\begin{cases} a_X = -\omega_e^2 x + \dfrac{\mu_e x}{r^3} \\ a_Y = 0 \\ a_Z = \dfrac{\mu_e z}{r^3} \end{cases} \tag{3}$$

Let us consider an inertial reference frame, $I\left(X^{(I)}, Y^{(I)}, Z^{(I)}\right)$, with the origin at the Earth's center; the $X^{(I)}$ axis is aligned with the projection of the Sun-Earth vector on the equatorial plane *at* winter solstice; the $Z_I$ axis is aligned with the angular momentum vector of the Earth and perpendicular to the equatorial plane, and the $Y^{(I)}$ axis completes the right-handed Cartesian reference frame. In that frame, the ideal DGEO is a circle with a constant radius from the $Z^{(I)}$ axis and at constant distance from the $X^{(I)}$-$Y^{(I)}$ plane, i.e. parallel to the equatorial plane (see Fig. 2). The magnitude and direction of the acceleration required to maintain the NKO are constant in frame (*A*), see Eq. (3), and therefore conduct a rotation once per DGEO period in frame (*I*), see the arrows in Fig. 2.

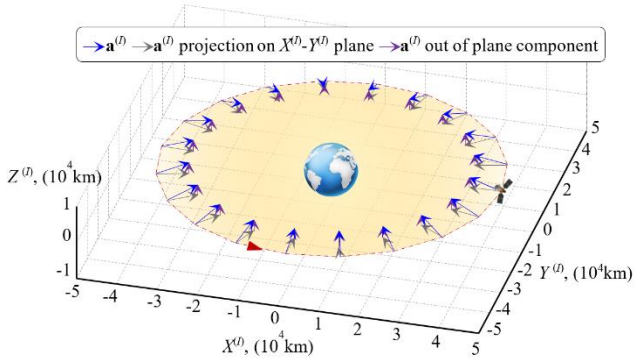


Fig. 2 Acceleration and trajectory over one day of a DGEO in the inertial reference frame (*I*)

A. Solar sail propulsion

Solar sails can produce continuous accelerations without any propellant consumption. In this work, a perfect solar sail force model will be used, which only accounts for specular reflection. Note that, in reality, the efficiency of the sail will be less than that of an ideal sail due to non-ideal reflecting and billowing effects. However, these effects are neglected for the current study.

The acceleration generated by an ideal solar sail can be modeled as

$$\mathbf{a}_S = \beta_0 \frac{m_0}{m} \frac{\mu_s}{s^2} (\hat{\mathbf{n}} \cdot \hat{\mathbf{s}})^2 \hat{\mathbf{n}} \tag{4}$$

where $\mu_s$ is the gravitational parameter of the Sun, $\hat{\mathbf{n}}$ is the vector normal to the sail surface, $\mathbf{s}$ is the Sun-sail vector, $\hat{\mathbf{s}}$ is the unit vector along $\mathbf{s}$, $m$ is the instantaneous mass of the spacecraft and $m_0$ is the initial mass.

Note that the ratio of $m_0$ and $m$ describes the decrease in the hybrid sail spacecraft mass due to the consumption of propellant by the SEP system (for a pure solar sail spacecraft this ratio equals 1).

In this work, $\|\mathbf{s}\|$ is approximated by a constant Sun-Earth distance of 1 astronomical unit (AU). The parameter $\beta_0$ is the system lightness number at the start of the mission, which can be defined as

$$\beta_0 = \sigma \frac{A}{m_0} \tag{5}$$

where $A$ is the solar sail area and $\sigma$ is the critical sail loading which equals $1.53\,\mathrm{g/m^2}$ in the solar system [3]. The analyses in this paper will be performed with a lightness number $\beta_0$ ranging from 0 (pure SEP) to 0.2. A value of $\beta_0 = 0.05$ can be assumed to be near-term solar sail technology [3].

Considering the tilt of the Earth's rotational axis with respect to the ecliptic plane, the direction of the Sun-sail vector $\mathbf{s}$ changes periodically. An Earth-fixed rotating reference frame, $B\left(X^{(B)}, Y^{(B)}, Z^{(B)}\right)$, which is shown in Fig. 3, is used to model this variation in $\mathbf{s}$. Reference frame ($B$) is centered at the Earth, with the $Z^{(B)}$ axis aligned with the angular momentum vector of the Earth and perpendicular to the equatorial plane, the $X^{(B)}$ axis aligned with the projection of the Sun-sail vector on the equatorial plane, and the $Y^{(B)}$ axis completes the right-handed Cartesian reference frame. Again, because the spacecraft-Earth distance is much smaller than the spacecraft-Sun distance, we neglect the tiny variation in the direction of the Sun-sail vector as the spacecraft orbits the Earth and assume it to be aligned with the Sun-Earth vector. Reference frame ($B$) rotates with the angular velocity of the Earth around the Sun, $\omega_s$, which ensures that the unit vector $\hat{\mathbf{s}}^{(B)}$ is always contained in the $X^{(B)}$-$Z^{(B)}$ plane. The angle $\psi$ is the angle between $\hat{\mathbf{s}}^{(B)}$ and the $X^{(B)}$ axis, which reaches its maximum value (equal to the Earth's obliquity to the ecliptic, $\delta$) at winter solstice and reaches its minimum value $-\delta$ at summer solstice. As the Earth orbits around the Sun, the angle $\chi$ describes the position of the Earth in the inertial reference frame ($I$), as

$$\chi = \omega_s t \tag{6}$$

where $t$ is the time since winter solstice (see Fig. 4). The angle $\psi$ is a function of $\chi$ [1]:

$$\psi(\chi) = \sin^{-1}(\sin\delta\cos\chi) \tag{7}$$

and obtains its maximum value at winter solstice when $\psi(0) = \delta$, and its minimum value at summer solstice when $\psi(\pi) = -\delta$ [1]. Then, the relationship between $\psi$ and $t$ can be written as

$$\psi(t) = \sin^{-1}(\sin\delta\cos\omega_s t) \tag{8}$$

According to Eq. (8), $\psi$ can be uniquely determined from the time $t$, yielding

$$\hat{\mathbf{s}}^{(B)} = \left[\cos\psi \;\; 0 \;\; \sin\psi\right]^{\mathrm{T}} \tag{9}$$

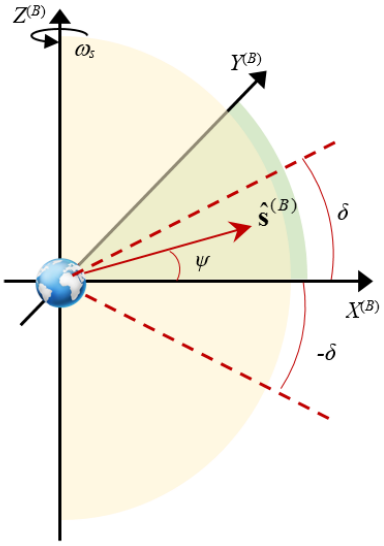


Fig. 3 Frame ($B$) used to model the cyclical change of the Sun-sail direction $\hat{\mathbf{s}}^{(B)}$

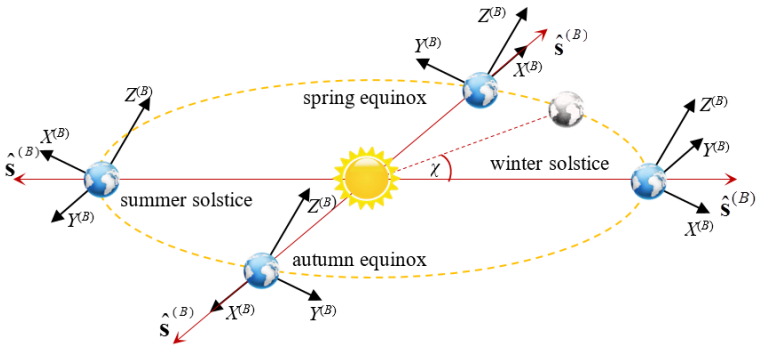


Fig. 4 Frame ($B$) and Sun-sail direction $\hat{\mathbf{s}}^{(B)}$ over one year

Considering the attitude constraint of the solar sail that $\hat{\mathbf{n}}$ cannot point towards the Sun, a reference frame ($C$) is used to model the control pitch angle $\alpha$ and yaw angle $\theta$ of the solar sail. In reference frame ($C$), the $X^{(C)}$ axis coincides with the Sun-sail vector (again neglecting the tiny variation in the direction of the Sun-sail vector over one orbit, assuming it to be aligned with the Sun-Earth vector), the $Z^{(C)}$ axis is perpendicular to the $X^{(C)}$ axis and lies in the plane spanning the Sun-sail vector and the Earth's rotation axis, and the $Y^{(C)}$ axis completes the right-handed

reference frame (see Fig. 5). Then, the unit vector $\hat{\mathbf{n}}$ can be described as

$$\hat{\mathbf{n}}^{(C)}=[\sin\alpha\cos\theta \;\; \sin\alpha\sin\theta \;\; \cos\alpha]^{\mathrm{T}} \tag{10}$$

Because $\hat{\mathbf{n}}^{(C)}$ should always point away from the Sun, in frame ($C$) the following attitude constraints on $\alpha$ and $\theta$ apply:

$$\begin{cases} 0 \le \alpha \le \pi \\ -\dfrac{\pi}{2} \le \theta \le \dfrac{\pi}{2} \end{cases} \tag{11}$$

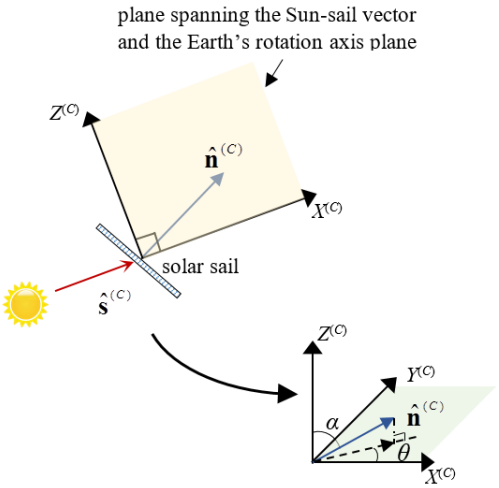


Fig. 5 Frame ($C$) with sail normal $\hat{\mathbf{n}}$, pitch angle $\alpha$ and yaw angle $\theta$

Through a rotation around the $Y^{(C)}$ axis over an angle $-\psi$, frame ($C$) will coincide with frame ($B$). Hence, the rotation matrix $\mathbf{R}_{C\to B}$ between those two frames is:

$$\mathbf{R}_{C\to B}=\begin{bmatrix} \cos(-\psi) & 0 & -\sin(-\psi) \\ 0 & 1 & 0 \\ \sin(-\psi) & 0 & \cos(-\psi) \end{bmatrix} \tag{12}$$

which yields

$$\hat{\mathbf{n}}^{(B)}=\mathbf{R}_{C\to B}\hat{\mathbf{n}}^{(C)} \tag{13}$$

Furthermore, the rotation matrix $\mathbf{R}_{B\to A}$ between frame ($B$) and frame ($A$) can be described as

$$\mathbf{R}_{B\to A}=\begin{bmatrix} \cos\zeta & \sin\zeta & 0 \\ -\sin\zeta & \cos\zeta & 0 \\ 0 & 0 & 1 \end{bmatrix} \tag{14}$$

where the rotating angle $\zeta$ is given by

$$\zeta = L+\mathrm{mod}(t,T_{GEO})\omega_e-\chi \tag{15}$$

In Eq. (15), $T_{\mathrm{GEO}}$ is the orbital period of the (displaced) GEO, i.e. one day. Furthermore, the parameter $L$ is included because the GEO spacecraft can be positioned at any longitude. Note that, for $L=0$ the frames ($A$) and ($B$) coincide at winter solstice (see Fig. 6).

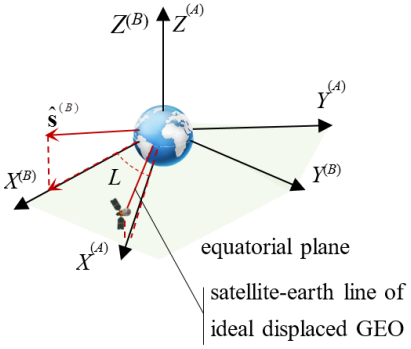


Fig. 6 Angle correction $L$ in frame ($A$) for ideal DGEO at winter solstice

Then, $\hat{\mathbf{n}}$ and $\hat{\mathbf{s}}$ are given by

$$\begin{cases}\hat{\mathbf{n}}=\mathbf{R}_{B\to A}\hat{\mathbf{n}}^{(B)}\\ \hat{\mathbf{s}}=\mathbf{R}_{B\to A}\hat{\mathbf{s}}^{(B)}\end{cases} \tag{16}$$

Substituting Eq. (16) into Eq. (4) allows $\mathbf{a}_{\mathrm{S}}$ to be computed.

B. Solar electric propulsion

We assume an ideal SEP thruster that can be tilted in any direction and can provide an adjustable thrust up to a maximum thrust $f_{\max}$. In frame ($A$), the thrust vector of the SEP thruster $\mathbf{f}_{\mathrm{SEP}}$ can be written as

$$\mathbf{f}_{\mathrm{SEP}}=[\,f_X \quad f_Y \quad f_Z\,]^{\mathrm{T}} \tag{17}$$

The magnitude of the SEP thrust vector is defined as $f=\left\|\mathbf{f}_{\mathrm{SEP}}\right\|$, which is modeled as

$$f=-\dot{m}I_{\mathrm{SP}}g_0 \tag{18}$$

where $\dot{m}$ is the rate of change of the spacecraft mass, $I_{\mathrm{SP}}$ is the specific impulse and $g_0$ is the standard Earth surface gravity acceleration. A specific impulse of $I_{\mathrm{SP}}=3200\,\mathrm{s}$ can be assumed using current engine technology [31,32]. Considering the assumed capabilities of the SEP thruster, the following magnitude constraint for $f$ applies:

$$0\le f\le f_{\max} \tag{19}$$

Then, $\mathbf{a}_{\mathrm{SEP}}$ can be obtained according to

$$\mathbf{a}_{\mathrm{SEP}}=\frac{\mathbf{f}_{\mathrm{SEP}}}{m} \tag{20}$$

Finally, by introducing the velocity vector $\mathbf{v}=\dot{\mathbf{r}}=[v_X \;\; v_Y \;\; v_Z]^{\mathrm{T}}$, the differential equations of the state vector $\mathbf{S}$ of the hybrid sail spacecraft can be written as

$$\dot{\mathbf{S}}=[\dot{\mathbf{r}} \;\; \dot{\mathbf{v}} \;\; \dot{m}]^{\mathrm{T}} \tag{21}$$

And then, the first-order form of Eq. (21) can be found by substituting Eq. (1) and Eq. (18)

$$\begin{bmatrix} \dot{x} \\ \dot{y} \\ \dot{z} \\ \dot{v}_X \\ \dot{v}_Y \\ \dot{v}_Z \\ \dot{m} \end{bmatrix} = \begin{bmatrix} v_X \\ v_Y \\ v_Z \\ 2\omega_e v_Y + \omega_e{}^2 x - \dfrac{\mu_e x}{r^3} + a_{\mathrm{S},X} + a_{\mathrm{SEP},X} \\ -2\omega_e v_X + \omega_e{}^2 y - \dfrac{\mu_e y}{r^3} + a_{\mathrm{S},Y} + a_{\mathrm{SEP},Y} \\ -\dfrac{\mu_e z}{r^3} + a_{\mathrm{S},Z} + a_{\mathrm{SEP},Z} \\ \dfrac{-f}{I_{\mathrm{SP}} g_0} \end{bmatrix} \tag{22}$$

## III. Displaced Geostationary Orbit Design

In frame ($A$), the GEO is a static point along the $X$ axis, at a distance $r_{\mathrm{GEO}}$ from the origin (see Fig. 7) and describes a perfect circle in the Earth-centered inertial reference frame ($I$). An ideal DGEO is defined as a spacecraft that is constantly aligned with a certain point on the Earth which is not necessarily confined to the equator. Then, the ideal DGEO is an equilibrium point in the $X$-$Z$ plane of frame ($A$), that has an offset along the $X$ axis with respect to the GEO of $d_X$ and similar for $d_Y$ ($d_Y$=0) and $d_Z$ (see Fig. 7). Finally, by defining a station-keeping box around the ideal DGEO equilibrium point, the LDGEOs are obtained. In this section, minimum-propellant ideal- and loosely DGEOs will be designed by solving an optimal control problem with a Gauss-pseudospectral algorithm, which is sensitive to the initial guess for strongly non-linear optimization problems. Therefore, as described in the following subsection, we use an inverse method on the ideal DGEOs to create a close-enough sub-optimal initial guess to allow the Gauss-pseudospectral algorithm to converge quickly and smoothly to a locally-optimal solution for the LDGEOs.

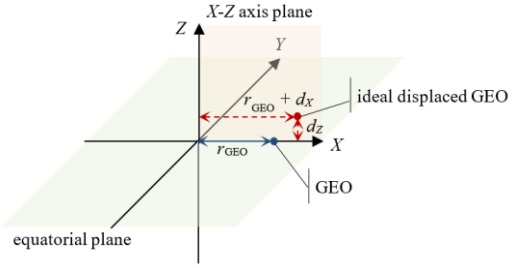


Fig. 7 GEO and DGEO location in frame ($A$)

A. Ideal displaced GEO

The daily rotation period of the Earth is much shorter than its yearly revolution about the Sun. Hence, there is no need to consider the change of Sun direction within a daily cycle and it is reasonable to design a one-day periodic DGEO and maintain it as long as the direction of the Sun-sail vector does not change significantly. Therefore, the dynamics of the spacecraft are constrained to follow the self-rotation of the Earth. Assuming that the initial time $t_0 = 0$ coincides with the winter solstice when $\chi = 0$ and $\psi = \delta$, in frame ($A$), the state of the spacecraft at any generic instant of time $t$ can be written as

$$\mathbf{r}(t) = \begin{bmatrix} r_{\mathrm{GEO}} + d_{\mathrm{X}} \\ 0 \\ d_{\mathrm{Z}} \end{bmatrix}$$
$$\dot{\mathbf{v}}(t) = \mathbf{v}(t) = \begin{bmatrix} 0 \\ 0 \\ 0 \end{bmatrix} \tag{23}$$

Substituting Eq. (23) into Eq. (22) and rearranging gives the required acceleration for an ideal DGEO (indicated by subscript 'I'):

$$\mathbf{a}_{\mathrm{I}} = \begin{bmatrix} -\omega_e{}^2 (r_{GEO} + d_X) + \dfrac{\mu_e (r_{GEO} + d_X)}{\sqrt{(r_{GEO} + d_X)^2 + d_Z{}^2}^3} \\ 0 \\ \dfrac{\mu_e d_Z}{\sqrt{(r_{GEO} + d_X)^2 + d_Z{}^2}^3} \end{bmatrix} \tag{24}$$

From Eq. (2) it then follows that:

$$\mathbf{a}_{\mathrm{SEP}} = \mathbf{a}_{\mathrm{I}} - \mathbf{a}_{\mathrm{S}}(\alpha_{\mathrm{I}}, \theta_{\mathrm{I}}) \tag{25}$$

Inspecting Eq. (25), for any given $m$ and $t$, $\mathbf{a}_{\mathrm{SEP}}$ is a function of $\alpha_{\mathrm{I}}$ and $\theta_{\mathrm{I}}$. Then, the optimal pitch angle $\alpha_{\mathrm{I}}^*$

and yaw angle $\theta_{\mathrm{I}}^{*}$ for the ideal DGEO can be found by minimizing the SEP propellant at each instant of time.

$$(\alpha_{\mathrm{I}}^{*}(t),\theta_{\mathrm{I}}^{*}(t))=\arg\min_{\substack{\alpha\in[0,\pi]\\ \theta\in[-\pi/2,\pi/2]}}(\|\mathbf{a}_{\mathrm{SEP}}(t)\|) \tag{26}$$

Equation (26) is solved using MATLAB's genetic algorithm toolbox. Once $\alpha_{\mathrm{I}}^{*}$ and $\theta_{\mathrm{I}}^{*}$ are found, the optimal accelerations $\mathbf{a}_{\mathrm{S}}^{*}(t)$, $\mathbf{a}_{\mathrm{SEP}}^{*}(t)$ can be obtained, as well as the optimal $m^{*}(t)$, for any specific DGEO. Furthermore, for multi-revolutions of the DGEO, this method can be repeated for each day. For this, we define the initial time of the $i^{\mathrm{th}}$ day, $t_i$ $(i=0,1,2...)$, as $t_{i+1}=t_i+T_{GEO}$. Discretizing the DGEO into $n$ nodes, the time at each node $j$ can be written as

$$t_{ij}=t_i+\frac{(j-1)T_{GEO}}{n}\quad(j=1,2,...n) \tag{27}$$

where $t_{ij}$ indicates the time at the $j^{\mathrm{th}}$ node of the $i^{\mathrm{th}}$ orbit since winter solstice. The corresponding mass $m_{ij}$ at each point can be defined as

$$m_{ij}=m_{i0}-\sum_{k=1}^{j}\frac{T_{GEO}f_{ik}^{*}}{nI_{SP}g_0}\quad(j=1,2,...n) \tag{28}$$

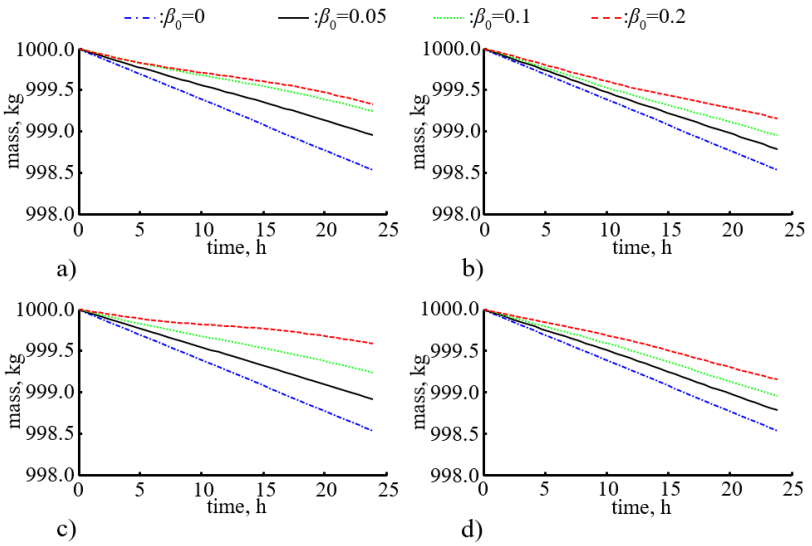


Fig. 8 Ideal DGEO: mass trends at a) winter solstice b) spring equinox c) summer solstice d) autumn equinox for different values of $\beta_0$ with $m_{i0}=1000$ kg, $d_X=5$ km, $d_Y=0$ km and $d_Z=100$ km.

where $m_{i0}$ $(i=0,1,2...)$ is the mass at the beginning of the $i^{\mathrm{th}}$ orbit and $f_{ik}^{*}$ is the optimized SEP thrust which can be obtained from Eq. (18) and Eq. (26). Details of the resulting ideal DGEOs and required solar sail and SEP accelerations can be found in [1]. Here, only a summarizing plot of the mass trend over 1 day is given in Fig. 8 for different

times during the year and for an initial mass of $m_{i0} = 1000$ kg and a DGEO defined by $d_X = 5$ km, $d_Y = 0$ km and $d_Z = 100$ km, for the sake of comparison with following results.

B. Optimal displaced GEO with loose position constraints

This section extends the analysis from the ideal DGEO to that of the LDGEO: the constraints of constant distance from the GEO through constant values for $d_X$, $d_Y$ and $d_Z$ are relaxed and the spacecraft is allowed to move freely within a station-keeping box. This box is defined as

$$K = \{x, y, z \mid x \in [r_{\text{GEO}} + d_X - \rho_X, r_{\text{GEO}} + d_X + \rho_X],\ y \in [d_Y - \rho_Y, d_Y + \rho_Y],\ z \in [d_Z - \rho_Z, d_Z + \rho_Z]\},\ (\rho_X, \rho_Y, \rho_Z \geq 0)$$

where $\rho_X$, $\rho_Y$ and $\rho_Z$ are relaxing parameters on $d_X$, $d_Y$ and $d_Z$. As a result, a set of LDGEOs can be obtained. In particular, in frame ($A$), the movement of the spacecraft is constrained to a control box whose volume is determined by $8\rho_X\rho_Y\rho_Z$. To avoid collisions with spacecraft in GEO, the following constraints are imposed on the station-keeping box:

$$\sqrt{(x - r_{\text{GEO}})^2 + (z)^2} \geq r_{\text{safe}},\ [x, y, z] \in K \tag{29}$$

where $r_{\text{safe}}$ is a large enough distance from the GEO.

The LDGEO optimization problem is that of finding periodic orbits that minimize the propellant consumption, while satisfying the station-keeping constraints. In this work, the dynamics are described by the differential equations in Eq. (22). As the problem is initially solved for one orbital period, the time constraints are:

$$t_{\text{ini}} = iT_{\text{GEO}},\quad t_{\text{fin}} = (i+1)T_{\text{GEO}} \quad (i = 0, 1, 2...) \tag{30}$$

where $t_{\text{ini}}$ is the initial time and $t_{\text{fin}}$ is the final time on the $i^{\text{th}}$ orbit. To minimize the propellant consumption, the cost function is

$$J = -m\left(t_{\text{fin}}\right) \tag{31}$$

which corresponds to maximizing the final mass after one orbit. In addition, since the spacecraft should stay in the station-keeping box at any time $t_{\text{ini}} \leq t \leq t_{\text{fin}}$, the following path constrains are defined:

$$\begin{cases} x(t) \in [r_{\text{GEO}} + d_X - \rho_X, r_{\text{GEO}} + d_X + \rho_X] \\ y(t) \in [d_Y - \rho_Y, d_Y + \rho_Y] \\ z(t) \in [d_Z - \rho_Z, d_Z + \rho_Z] \\ \sqrt{(x(t) - r_{\text{GEO}})^2 + z(t)^2} \geq r_{\text{safe}} \end{cases} \tag{32}$$

According to Eq. (17), the controls of the SEP thrust vector are described through the parameters $f_X$, $f_Y$ and $f_Z$, which require the definition of a path constraint on the thrust magnitude

$$\sqrt{f_X{}^2+f_Y{}^2+f_Z{}^2} \le f_{\max} \tag{33}$$

In addition, the solar sail force is controlled through the attitude angles $\alpha$ and $\theta$ with bounds on these angles in Eq.(11).

The above-mentioned optimal control problem is solved with a numerical direct pseudospectral method implemented in the software tool PSOPT [33]. PSOPT makes use of the automatic differentiation by overloading in C++ (ADOL-C) library for the automatic differentiation of the objective, dynamics, constraint functions and the initial guess for the problem.

The optimization is set-up for an LDGEO spacecraft trajectory at winter solstice ($L$=0, $\chi$=0 and $\psi = \delta$), for different values of $\beta_0$ and for $m_{i0}$=1000 kg, $f_{\max}$=0.6 N, $r_{\text{safe}}$=40km, $d_X$=5 km, $\rho_X$=10 km, $d_Y$=0 km, $\rho_Y$=10 km, $d_Z$=100 km, and $\rho_Z$=10 km.

The optimal trajectories of the spacecraft at winter solstice are shown in Fig. 9. It is obvious that the $X$- and $Z$-position components have some symmetrical features around time 12:00 (as seen in Fig. 9 (a) and (c)), and that the $Y$-position component is anti-symmetrical (Fig. 9 (b)). That is because at winter solstice, before 12:00 the spacecraft moves towards the Sun, and moves away from it after 12:00. Hence, neglecting the slight change of $\chi$ in a single day, the Sun-sail direction is approximately symmetrical around noon. However, although the Sun-sail vector is symmetrical, the velocity points towards the Sun before 12:00 and away from it after. This explains why the spacecraft velocities and accelerations along the orbit are not perfectly symmetrical/anti-symmetrical. Furthermore, for each position component, the curves for smaller values of $\beta_0$ such as 0 and 0.05 change gently, while the curves for larger values for $\beta_0$ such as 0.1 and 0.2 change more rapidly. Finally, there is a tendency for the $Z$ component of the optimal trajectories to be as close as possible to the equatorial plane to save propellant. Hence, the $Z$ component of optimal trajectories roughly coincide with the lower boundary of the station-keeping box. However, in all cases, the position of the spacecraft is strictly inside the station-keeping box, which verifies the effectiveness of the path constrains in Eq. (31).

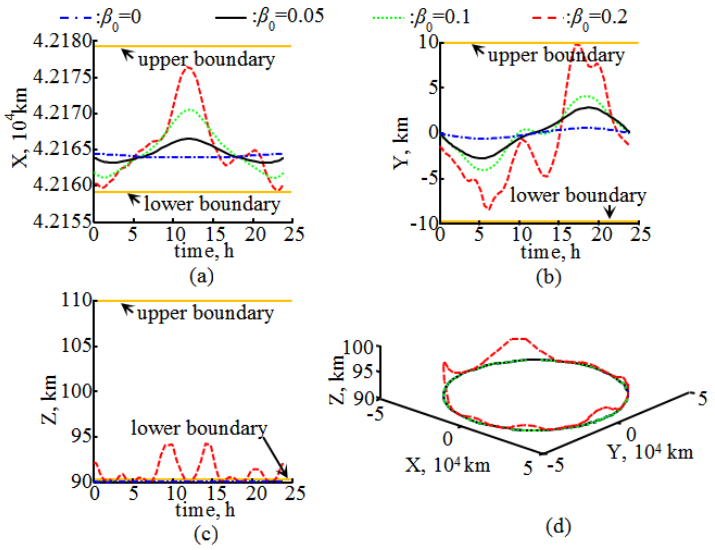


Fig. 9 LDGEO on winter solstice: a-c) spacecraft Cartesian position components in frame ($A$) d) Orbit in inertial reference frame ($I$) ($Z$-axis not to scale)

The acceleration required from the SEP thruster is plotted in Fig. 10. At winter/summer solstice, the thrust decreases at first and increases at the end of the day, while at spring/autumn equinox, the thrust decreases at first, begins to increase after 6:00, and then starts to decrease at 12:00 and increases again at 18:00. It is important to reiterate that the solar sail cannot generate a force component in the direction of the Sun. Hence, the solar sail performance is optimal when the Sun-sail vector coincides with the direction of acceleration needed to maintain the orbit. From Fig. 10 it is clear that, on winter/summer solstice, this occurs around noon as the SEP thrust is close to zero, which means that no propellant is consumed during that time span. Furthermore, the larger the value of $\beta_0$, the longer that time span is, which implies that more propellant is saved.

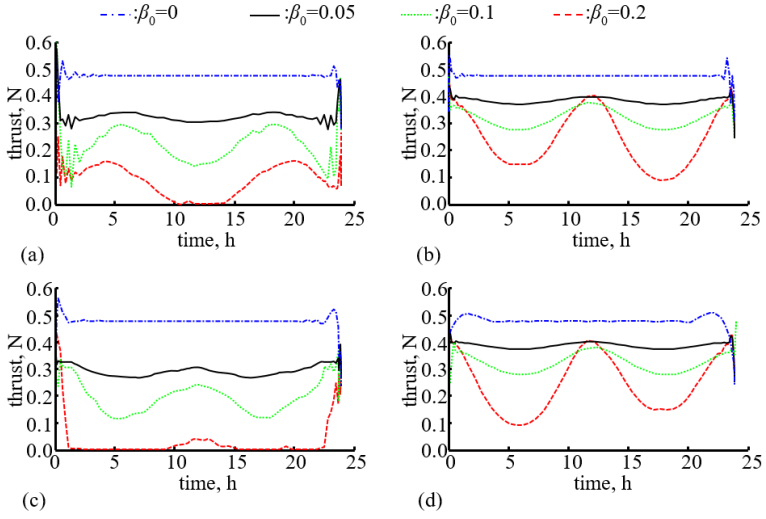


Fig. 10 LDGEO: SEP thrust magnitude at a) winter solstice b) spring equinox c) summer solstice d) autumn equinox

The control angles of the solar sail, $\alpha$ and $\theta$, are represented in Fig. 11 and must satisfy the constraints of Eq. (11). Note that, when any control angle reaches its limits ($\alpha \in [0^\circ, 180^\circ]$, $\theta \in [-90^\circ, 90^\circ]$), the sail is oriented parallel to the Sun-sail direction, creating no solar sail acceleration. This occurs for larger values of $\beta_0$, such as for $\beta_0 = 0.2$, to prevent the sail from generating a too large acceleration and thereby adversely affecting the SEP propellant consumption. Therefore, the control angles for large values of $\beta_0$ are adjusted more significantly than for small values of $\beta_0$ to obtain the most optimal coupled magnitude and direction of solar sail thrust.

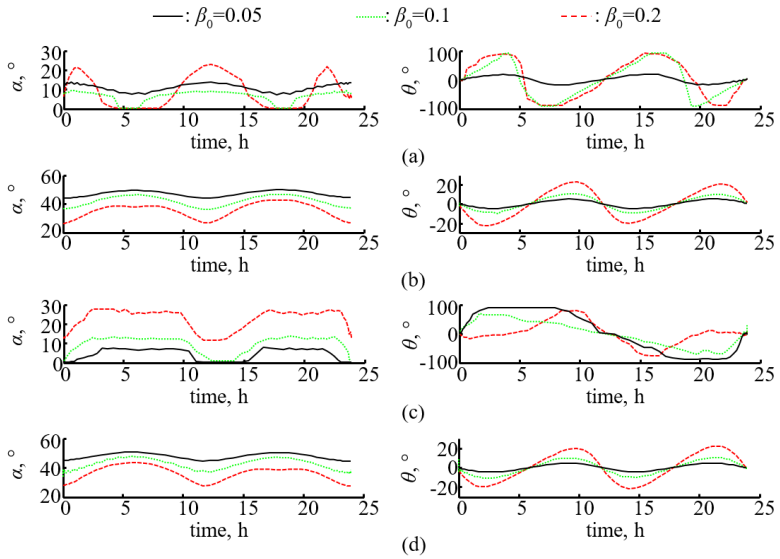


Fig. 11 LDGEO: solar sail control angles $\alpha$ and $\theta$ in frame ($C$) at a) winter solstice b) spring equinox c) summer solstice d) autumn equinox.

As an indication of the steering effort required from the solar sail, Fig. 12 presents the rates of change of the solar sail control angles $\alpha$ and $\theta$. For the angle $\alpha$, the maximum slew rate is smaller than $0.01^\circ/\mathrm{s}$, regardless of the time during the year. Instead, the maximum slew rate of the angle $\theta$ is relatively small at spring and autumn equinoxes (less than $0.01^\circ/\mathrm{s}$), but relatively large on winter and summer solstices at $0.1^\circ/\mathrm{s}$. This latter value may pose a challenge to very large sails. Future research will therefore investigate the inclusion of a constraint on the sail's maximum slew rate.

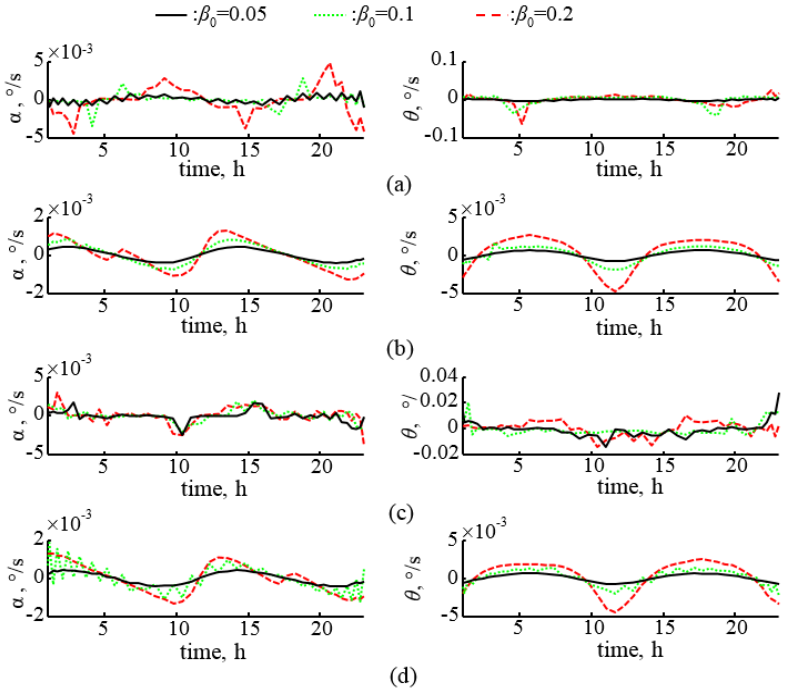


Fig. 12 LDGEO: rate of change of solar sail control angles $\alpha$ and $\theta$ at a) winter solstice b) spring equinox c) summer solstice d) autumn equinox

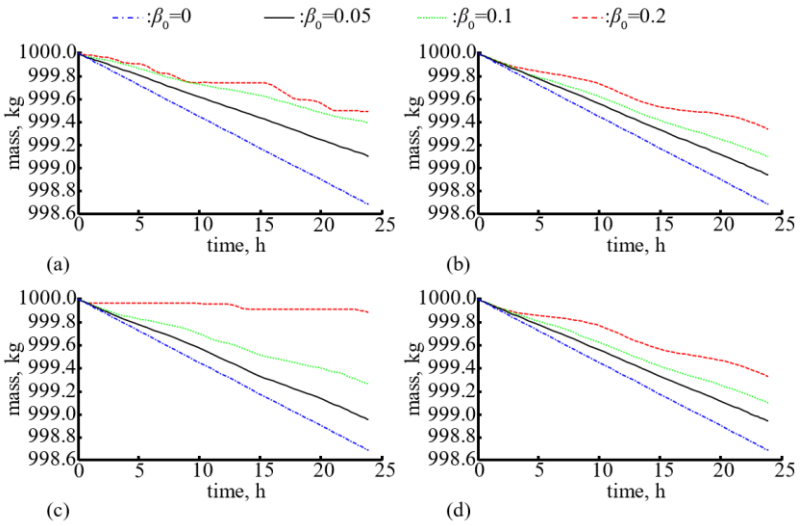


Fig. 13 LDGEO: spacecraft mass for different values of $\beta_0$ at a) winter solstice b) spring equinox c) summer solstice d) autumn equinox

Finally, the mass as a function of time appears in Fig. 13 (a-d) and a comparison between the ideal and loosely DGEOs is shown in Table 1. For a one-day orbit, the decrease in propellant consumption due to the loosening of the position constraint is obvious from Table 1. The relaxing of the orbital constraint clearly increases the effectiveness of

the solar sail: for the most favorable time of the year (at summer solstice) and for $\beta_0$=0.2 , the optimal trajectory with loose position constraints enables the hybrid sail to save up to 74% propellant mass compared to the ideal DGEO. In other cases, the propellant saving is not as significant, but still evident.

The introduction of a station-keeping box (and therefore relative motion of the spacecraft with respect to the ground station) may raise concerns on the trackability of the spacecraft from ground. Therefore, the magnitude of this relative velocity is shown in Fig. 14. Because the station-keeping box size is relatively small, the additional velocities are also small: their maximum values on winter solstice, spring equinox, summer solstice and autumn equinox are 2 m/s, 1.8 m/s, 2.9 m/s and 1.5 m/s respectively. As an additional measure of the degree in which the spacecraft is geostationary, we define the "stationary angle" as the angle between the Earth-spacecraft vector and the $X$ axis of Frame ($A$). For a traditional GEO, this stationary angle is always 0, while for an ideal DGEO, the stationary angle is constant. Instead, for the LDGEOs, the stationary angle on winter solstice, spring equinox, summer solstice and autumn equinox is shown in Fig. 15. Even for the worst case ($\beta_0$ = 0.2), the stationary angle stays within a 0.01° interval, which is assumed to be an acceptable level. Finally, note that the assumed size of the station-keeping box is smaller than those used for current geostationary spacecraft [34,35]. The relative velocities shown in Fig. 14 and variations in the stationary angles in Fig. 15 are therefore not expected to impose any tracking difficulties.

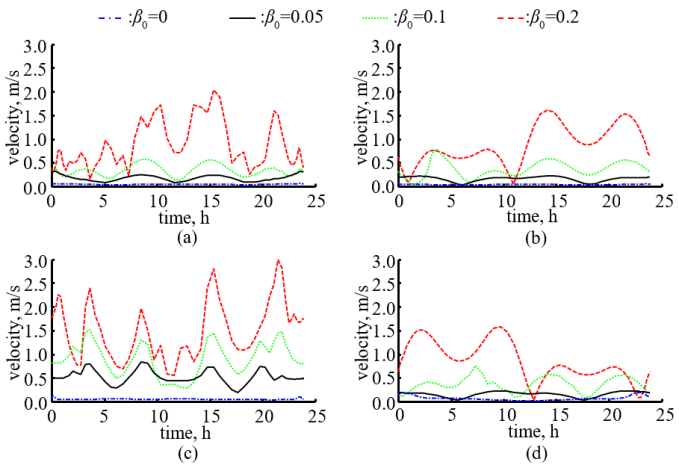


Fig. 14 LDGEO: spacecraft velocities in frame ($A$) at a) winter solstice b) spring equinox c) summer solstice d) autumn equinox

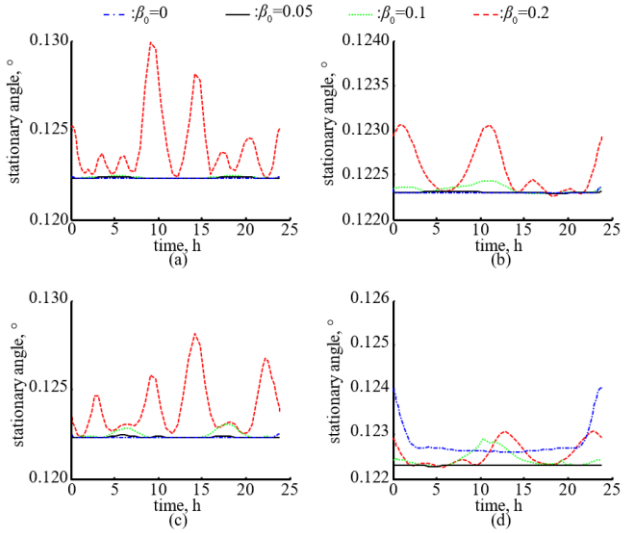


Fig. 15 LDGEO: stationary angle at a) winter solstice b) spring equinox c) summer solstice d) autumn equinox

The comparisons of final mass after one day for the ideal DGEO and the LDGEO are presented in Fig. 16. It is clear that the final mass initially increases as the value of $\beta_0$ increases. However, the relative increase is much larger for small values of $\beta_0$, i.e., for $\beta_0 < 0.3$. In fact, for a given DGEO, the extra solar sail acceleration due to a larger value of $\beta_0$ is not always beneficial from a propellant consumption perspective, and instead there is an optimal value of $\beta_0$ that minimizes it. For the ideal DGEO, as Fig. 16 (a) shows, the optimal $\beta_0$ is approximately 0.2 on winter solstice and approximately 0.4 on summer solstice. For the LDGEO, these values are 0.41 and 0.31, respectively.

Table 1 Comparison of propellant consumption between the ideal DGEO and LDGEOs

| day | $\beta_0$ | ideal DGEO (kg) | | LDGEO (kg) | | propellant saving (%) |
|---|---|---|---|---|---|---|
| | | final mass | propellant consumption | final mass | Propellant consumption | |
| winter solstice | 0.00 | 998.52 | 1.48 | 998.69 | 1.31 | 11 |
| | 0.05 | 998.95 | 1.05 | 999.10 | 0.90 | 14 |
| | 0.10 | 999.25 | 0.75 | 999.39 | 0.61 | 19 |
| | 0.20 | 999.32 | 0.68 | 999.49 | 0.51 | 25 |
| spring equinox | 0.00 | 998.52 | 1.48 | 998.69 | 1.31 | 11 |
| | 0.05 | 998.78 | 1.22 | 998.94 | 1.06 | 13 |
| | 0.10 | 998.95 | 1.05 | 999.10 | 0.90 | 14 |
| | 0.20 | 999.16 | 0.84 | 999.34 | 0.66 | 21 |
| summer solstice | 0.00 | 998.52 | 1.48 | 998.69 | 1.31 | 11 |
| | 0.05 | 998.91 | 1.09 | 999.00 | 1.00 | 8 |
| | 0.10 | 999.23 | 0.77 | 999.36 | 0.64 | 17 |
| | 0.20 | 999.58 | 0.42 | 999.89 | 0.11 | 74 |
| autumn equinox | 0.00 | 998.52 | 1.48 | 998.68 | 1.31 | 11 |
| | 0.05 | 998.78 | 1.22 | 998.94 | 1.06 | 13 |
| | 0.10 | 998.95 | 1.05 | 999.11 | 0.89 | 15 |
| | 0.20 | 999.15 | 0.85 | 999.30 | 0.70 | 18 |

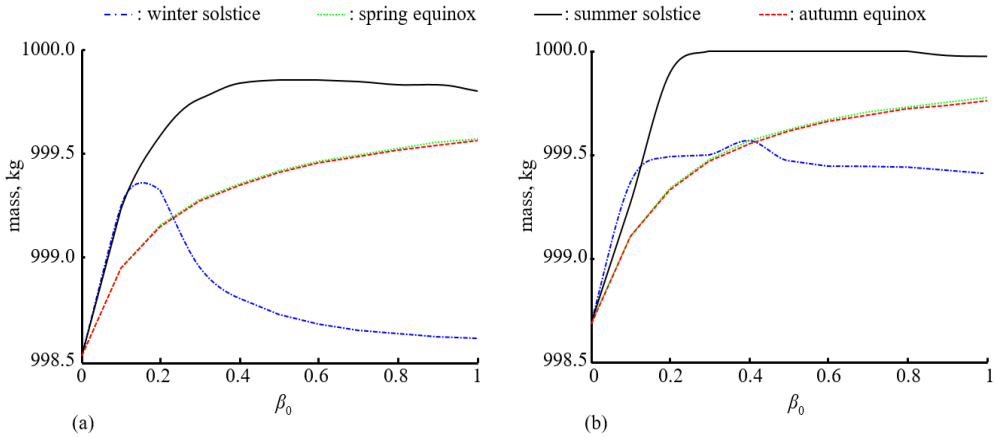


Fig. 16 Final mass after one day for a) ideal DGEO b) LDGEO

## IV. Mass Budget

In this work, the mass budget is based on the model proposed in [36]. The mass as a function of time can be expressed as:

$$m(t) = m_{\mathrm{PO}}(t) + m_{\mathrm{PT}} + m_{\mathrm{SEP}} + m_{\mathrm{GI}} + m_{\mathrm{SA}} + m_{\mathrm{S}} + m_{\mathrm{PL}} \tag{34}$$

where $m_{\mathrm{PO}}$ is the propellant mass which is also a function of time, $m_{\mathrm{PT}}$ is the mass of the propellant tank which is necessary to store the propellant, $m_{\mathrm{SEP}}$ is the mass of the SEP thruster which is a function of the maximum thrust required during the whole mission, and $m_{\mathrm{GI}}$ is the mass of the gimbal of the SEP thruster which is a function of $m_{\mathrm{SEP}}$. For a pure SEP spacecraft, an attitude maneuver or a simple gimbal are sufficient to enable thrust pointing. However, for a hybrid sail spacecraft, a relatively complex gimbal is needed to ensure the solar sail and SEP thruster can steer independently of each other. In Eq. (33), $m_{\mathrm{SA}}$ is the solar cell mass which is also a function of the maximum SEP thrust required during the whole mission. In this work, the pure SEP case is assumed to use a traditional solar array, while the hybrid sail case is assumed to use thin film solar cells which cover part of the sail. Finally, $m_{\mathrm{S}}$ is the mass of the solar sail and $m_{\mathrm{PL}}$ is the mass of the payload. The specific sub-items of Eq. (32) are given by [36]:

$$
\begin{aligned}
m_{\mathrm{PT}} &= \frac{m_{\mathrm{PO}}(t_0)}{10} \\
m_{\mathrm{SEP}} &= k_{\mathrm{SEP}} P_{\mathrm{SEP,\,max}} = \frac{k_{\mathrm{SEP}} f_{\max}^{'} I_{\mathrm{sp}} g_0}{2\eta_{\mathrm{SEP}}} \\
m_{\mathrm{SA}} &= \begin{cases} k_{\mathrm{SA}} P_{\mathrm{SEP,\,max}} = \dfrac{k_{\mathrm{SA}} f_{\max}^{'} I_{\mathrm{sp}} g_0}{2\eta_{\mathrm{SEP}}}, & \text{pure SEP} \\ \sigma_{\mathrm{TF}} A_{\mathrm{TF}} = \dfrac{\sigma_{\mathrm{TF}} f_{\max}^{'} I_{\mathrm{sp}} g_0}{2\eta_{\mathrm{SEP}} W \eta_{\mathrm{TF}} \cos\alpha_{f_{\max}^{'}}}, & \text{hybrid sail} \end{cases} \\
m_{\mathrm{GI}} &= \begin{cases} \dfrac{m_{\mathrm{SEP}}}{10} = \dfrac{k_{\mathrm{SEP}} f_{\max}^{'} I_{\mathrm{sp}} g_0}{20\eta_{\mathrm{SEP}}}, & \text{pure SEP} \\ \dfrac{3m_{\mathrm{SEP}}}{10} = \dfrac{3k_{\mathrm{SEP}} f_{\max}^{'} I_{\mathrm{sp}} g_0}{20\eta_{\mathrm{SEP}}}, & \text{hybrid sail} \end{cases} \\
m_{\mathrm{S}} &= \begin{cases} 0, & \text{pure SEP} \\ \sigma_{\mathrm{S}} A_{\mathrm{S}} = \sigma_{\mathrm{S}} \left( \dfrac{\beta_0 m_0}{\sigma} + \dfrac{f_{\max}^{'} I_{\mathrm{sp}} g_0}{2\eta_{\mathrm{SEP}} W \eta_{\mathrm{TF}} \cos\alpha_{f_{\max}^{'}}} \right), & \text{hybrid sail} \end{cases}
\end{aligned}
\tag{35}
$$

where $k_{\mathrm{SEP}}$ and $k_{\mathrm{SA}}$ are the SEP thruster and solar cell array performance coefficients, $P_{\mathrm{SEP,\,max}}$ is the maximum power required by the SEP thruster, $f_{\max}^{'}$ is the maximum SEP thrust magnitude during the whole mission, $W$ is the energy flux density of the Sun and $\alpha_{f_{\max}^{'}}$ is the pitch angle of the solar sail at the instant that $f_{\max}^{'}$ is required. Furthermore, $\eta_{\mathrm{SEP}}$ and $\eta_{\mathrm{TF}}$ are the efficiencies of the SEP thruster and the thin film solar cells, $\sigma_{\mathrm{TF}}$ and $\sigma_{\mathrm{S}}$ are the sail loading of the thin film solar cells and the solar sail, and $A_{\mathrm{TF}}$ and $A_{\mathrm{S}}$ are the area of the thin film solar cells and the solar sail.

Compared to the pure SEP system, the hybrid system inevitably brings some additional complexity and corresponding mass. The goal of the mass budget is to find the smallest initial mass $m(t_0) = m_0$ for a given $m_{\mathrm{PL}}$ and mission time $[\,t_0\,, t_f\,]$. For the sake of comparison, the mass budget will be considered for both the hybrid sail spacecraft and the pure SEP spacecraft. To ensure that the spacecraft can maintain the optimal LDGEO, $m_{\mathrm{PO}}\left(t_f\right) \geq 0$ must be satisfied. Furthermore, substituting Eq. (35) into Eq. (34), and rearranging gives

$$
m_0 = \begin{cases} \dfrac{11\sigma}{10(\sigma\text{-}\sigma_{\mathrm{S}}\beta_0)} m_{\mathrm{PO}}(t_0) + \dfrac{\sigma}{(\sigma\text{-}\sigma_{\mathrm{S}}\beta_0)} m_{\mathrm{PL}} + \dfrac{f_{\max}^{'} I_{\mathrm{sp}} g_0 \sigma}{2\eta_{\mathrm{SEP}}(\sigma\text{-}\sigma_{\mathrm{S}}\beta_0)} \left( \dfrac{13k_{\mathrm{SEP}}}{10} + \dfrac{\sigma_{\mathrm{TF}} + \sigma_{\mathrm{S}}}{W\eta_{\mathrm{TF}} \cos\alpha_{T_{\max}}} \right), & \text{hybrid sail} \\ \dfrac{11}{10} m_{\mathrm{PO}}(t_0) + m_{\mathrm{PL}} + \dfrac{11k_{\mathrm{SEP}} + 10k_{\mathrm{SA}}}{20\eta_{\mathrm{SEP}}} f_{\max}^{'} I_{\mathrm{sp}} g_0, & \text{pure SEP} \end{cases}
\tag{36}
$$

To simplify the expression of $m_0$ in Eq. (34), we define $K_1$ and $K_2$ as follows:

$$K_1 = \frac{\sigma}{(\sigma - \sigma_S \beta_0)}$$
$$K_2 = \frac{f'_{\max} I_{sp} g_0 \sigma}{2\eta_{SEP}(\sigma - \sigma_S \beta_0)} \left( \frac{13 k_{SEP}}{10} + \frac{\sigma_{TF} + \sigma_S}{W \eta_{TF} \cos \alpha_{T_{\max}}} \right) \tag{37}$$

Then, for the hybrid sail, $m_0$ can be written as:

$$m_0 = 1.1 K_1 m_{PO}(t_0) + K_1 m_{PL} + K_2 \tag{38}$$

For current technology, realistic values for the different parameters appearing in Eq. (35) are shown in Table 2. Furthermore, based on solar sail technology development, realistic near-term and far-term values for $\sigma_S$ are shown in Table 3.

Table 2 Reference values of different parameters in the mass budget [31,37-39]

| $k_{SA}$ | $k_{SEP}$ | $I_{sp}$ | $g_0$ | $\sigma_{TF}$ | $W$ | $\eta_{TF}$ | $\eta_{SEP}$ | $\sigma^*$ |
|---|---|---|---|---|---|---|---|---|
| 0.022 kg/W | 0.02 kg/W | 3200 s | 9.81 m/s$^2$ | 0.1 kg/m$^2$ | 1367 W/m$^2$ | 0.05 | 0.7 | 1.53 g/m$^2$ |

Table 3 Value of $\sigma_S$ for different solar sail technology levels [3]

| near-term | far-term | future |
|---|---|---|
| 7.5 g/m$^2$ | 5 g/m$^2$ | 2 g/m$^2$ |

The smallest initial mass to carry a certain payload for a number of years, $m_0^*$, can be obtained by solving Eq. (35) with an iterative method. The optimal orbit is computed for each day during the year by repeatedly solving the optimal control problem with the method described in Section III.B, and updating the Sun-sail direction at the start of each day. Furthermore, the initial states of one day's trajectory match the final states of the previous day. According to Eq. (37), for a specific hybrid sail, the value of $K_1$ is fixed. Once $m_{PO}(t_0)$ and $m_{PL}$ are fixed, the value of $K_2$ will be fixed too. Hence, if the optimal $m_{PO}(t_0)$ is found, the $m_0^*$ will be found too. With an initial guess for the initial propellant mass, $m_{PO,0}(t_0)$, the optimal trajectory for a multi-year mission can be obtained by repeated optimization runs. The values of the $i^{th}$ solution, $m_{PO,i}(t_0)$ and $m_{PO,i}(t_f)$, are computed to update the value of the $i$+1$^{th}$ initial guess $m_{PO,i+1}(t_0) = m_{PO,i}(t_0) - m_{PO,i}(t_f)$ for the next iteration until the initial mass does not change by more than $10^{-1}$ kg. Tables 4-6 show the mass budgets for two mission scenarios: a 1-year mission and a 3-year mission, with three types of solar sails (a near term sail, a far-term sail and an imaginary future sail whose value for $\sigma_S$ equals 2 g/m$^2$) and two different orbits (an ideal DGEO and an optimal LDGEO). For ease of comparison, the payload mass has the same value in all cases, $m_{PL}$ = 100 kg, and different values for $\beta_0$ are also taken into consideration.

For the case of a near-term sail, the results are shown in Table 4. The pure SEP ( $\beta_0$ = 0) spacecraft requires $m_0^*$ = 1370.5 kg (for 1 year) and $m_0^*$ = 17877.0 kg (for 3 years) at injection into the ideal DGEO, while the optimal LDGEO only requires $m_0^*$ = 1180.7 kg (for 1 year) and $m_0^*$ = 9843.2 kg (for 3 years). This gives a first indication of the benefit of the LDGEO compared to the ideal DGEO. For the hybrid sail cases, according to Eq. (37), there is a strong and positive correlation between the value of $m_0$ and the values of $K_1$ and $K_2$. In addition, the value of $m_{\mathrm{PO}}(t_f)$ should be greater than or equal to zero. Hence, with that constraint, if the values of $K_1$ and $K_2$ are too large, Eq. (37) does not have a valid solution. This occurs for a 1-year mission for $\beta_0$ = 0.2 ( $K_1$ = 51.0) and for all hybrid 3-year missions. For the cases where a solution does exist (1-year mission and $\beta_0$=0.05 and $\beta_0$=0.1), the optimal LDGEO again provides significant savings in the initial mass (938.7 kg and 2274.8 kg, respectively). However, all initial masses for the hybrid case are larger than for the pure SEP case. This means that, for near-term solar sail technology, the weight of the solar sail makes the hybrid propulsion system uneconomic.

Table 4 Mass budget for near-term solar sail ( $\sigma_S$ = 7.5 g/m$^2$)

| | $t_f$, y | 1 | 1 | 1 | 1 | 3 | 3 | 3 | 3 |
|---|---|---|---|---|---|---|---|---|---|
| | $\beta_0$ | 0.0 | 0.05 | 0.1 | 0.2 | 0.0 | 0.05 | 0.1 | 0.2 |
| | $K_1$ | -- | 1.325 | 1.962 | 51.0 | -- | 1.325 | 1.962 | 51.0 |
| Ideal DGEO | $K_2$, kg | -- | 981.8 | 314.6 | -- | -- | -- | -- | -- |
| | $m_0^*$, kg | 1370.5 | 2269.5 | 4890.3 | -- | 17877.0 | -- | -- | -- |
| LDGEO | $K_2$, kg | -- | 531.3 | 1778.7 | -- | -- | 5990.9 | -- | -- |
| | $m_0^*$, kg | 1180.7 | 1330.8 | 2615.5 | -- | 9843.2 | 14470.6 | -- | -- |
| Mass saving, kg | | 189.8 | 938.7 | 2274.8 | -- | 8033.8 | -- | -- | -- |

Similar analyses are carried out for the far-term solar sail and the results are shown in Table 5. Again, the values of $m_0^*$ for the hybrid case and LDGEO are smaller than those for the ideal DGEO and are in this case also smaller than for the pure SEP case. Therefore, for a relatively small value of $\sigma_S$, the hybrid sail is effective. For future sail technology ( $\sigma_S$ =2 g/m$^2$), the results of the mass budget analysis are shown in Table 6. The small value for $\sigma_S$ makes $K_1$ less sensitive to the value of $\beta_0$. Hence, $K_1$ remains small for relative large values for $\beta_0$ and the hybrid sail, optimal LDGEOs can again achieve significant mass savings with respect to the SEP case and the ideal DGEO, especially for long duration missions.

Table 5 Mass budget for far-term solar sail ( $\sigma_S$ = 5 g/m$^2$)

| $t_f$, y | 1 | 1 | 1 | 1 | 3 | 3 | 3 | 3 |
|---|---|---|---|---|---|---|---|---|

| | | | | | | | | | |
|---|---|---|---|---|---|---|---|---|---|
| | $\beta_0$ | 0.0 | 0.05 | 0.1 | 0.2 | 0.0 | 0.05 | 0.1 | 0.2 |
| | $K_1$ | -- | 1.195 | 1.485 | 2.887 | -- | 1.195 | 1.485 | 2.887 |
| Ideal DGEO | $K_2$ ,kg | -- | 763.7 | 583.8 | -- | -- | 9668.0 | 4290.7 | -- |
| | ,kg | 1370.5 | 1440.2 | 1233.0 | -- | 17877.0 | 19577.7 | 9762.2 | -- |
| LDGEO | $K_2$ ,kg | -- | 372.5 | 433.1 | -- | -- | 3944.1 | 4209.7 | -- |
| | $m_0^*$,kg | 1180.7 | 972.3 | 877.1 | -- | 9843.2 | 9266.6 | 8871.2 | -- |
| Mass saving, kg | | 189.8 | 467.9 | 355.9 | -- | 8033.8 | 10311.1 | 891.0 | -- |

Table 6 Mass budget for future solar sail ( $\sigma_S$ = 2 g/m$^2$)

| | | | | | | | | | |
|---|---|---|---|---|---|---|---|---|---|
| | $t_f$ , y | 1 | 1 | 1 | 1 | 3 | 3 | 3 | 3 |
| | $\beta_0$ | 0.0 | 0.05 | 0.1 | 0.2 | 0.0 | 0.05 | 0.1 | 0.2 |
| | $K_1$ | -- | 1.070 | 1.150 | 1.354 | -- | 1.070 | 1.150 | 1.354 |
| Ideal DGEO | $K_2$ ,kg | -- | 359.4 | 300.9 | 376.3 | -- | 2289.5 | 1981.8 | 2567.9 |
| | $m_0^*$,kg | 1370.5 | 1022.4 | 822.2 | 850.5 | 17877. $m_0^*$0 | 6289.3 | 5001.0 | 5899.2 |
| LDGEO | $K_2$ ,kg | -- | 357.2 | 277.4 | 280.4 | -- | 2020.2 | 734.8 | 788.8 |
| | $m_0^*$,kg | 1180.7 | 812.3 | 720.5 | 642.1 | 9843.2 | 5697.2 | 2104.4 | 1800.7 |
| Mass saving, kg | | 189.8 | 210.1 | 101.7 | 208.4 | 8033.8 | 592.1 | 2896.6 | 4098.5 |

## V. Conclusions

In this paper, the concept of loosely-displaced geostationary orbits (GEOs) using a hybrid (solar sail and solar electric propulsion, SEP) propulsion system is proposed as a solution to the congestion of the GEO. This concept loosens the strict steady position constraint of the previously-introduced displaced GEO such that the spacecraft is now free to move within an assigned station-keeping box. Furthermore, by using hybrid sail propulsion instead of pure SEP, the spacecraft will consume less propellant to maintain the orbit. For a 10×10×10 km$^3$ station-keeping box around a displaced GEO 5 km outside and 100 km above the nominal GEO, the propellant mass needed to maintain the orbit for 1 day at summer solstice is 1.31 kg and 0.11 kg for the pure SEP and the hybrid sail (with a lightness number of 0.2), respectively. Smaller mass savings are observed for the case of no station-keeping box, which shows that the loosely-displaced GEO can more effectively exploit the contribution of the solar sail than the ideal displaced GEO. Furthermore, the mass budgets for a fixed payload mass and a given mission duration show that for sufficiently small sail mass-to-area ratios, the hybrid sail configuration requires smaller initial masses than the SEP configuration and that the loosely-displaced GEO can provide even more mass savings than the ideal displaced GEO, especially for long–duration missions.

## Acknowledgements

Yuan Liu would like to acknowledge the University of Glasgow for supporting his academic visit; The National

High Technology Research and Development Program of China (No. 2013AA122904); This research was jointly funded by the China Natural Science Foundation (No. 61633008).

Jeannette Heiligers acknowledges the support of the Marie Skłodowska-Curie Individual Fellowship 658645 - S4ILS: Solar Sailing for Space Situational Awareness in the Lunar System.

## References

1. Heiligers, J., Ceriotti, M., McInnes, C. R., and Biggs, J. D., "Displaced geostationary orbit design using hybrid sail propulsion," *Journal of Guidance*," *Control, and Dynamics*. 2011; 34(6): 1852-1866.
2. Mckay, R., Macdonald, M., Biggs, J. and McInnes, C., "Survey of highly non-Keplerian orbits with low-thrust propulsion," *Journal of Guidance, Control and Dynamics*, 2011; 34 (3): 645-666.
3. Ceriotti, M., Heiligers, J., and McInnes, C. R., "Trajectory and spacecraft design for a pole-sitter mission," *Journal of Spacecraft and Rockets*. 2014; 51(1): 311-326.
4. Heiligers, J., Ceriotti, M., McInnes, C. R., and Biggs, J. D., "Design of optimal transfers between North and South Pole-sitter orbits," *In: 22nd AAS/AIAA Space Flight Mechancis Meeting*, Charleston, SC, USA, 2012; 897-916.
5. Ozimek, M.T., Grebow, D.J., and Howell, K.C., "Design of solar sail trajectories with applications to lunar south pole coverage," *Journal of Guidance, Control, and Dynamics*, 2009; 32(6): 1884-1897.
6. Simo, J., and McInnes, C. R., "Designing displaced lunar orbits using low-thrust propulsion," *Journal of Guidance, Control, and Dynamics*, 2010; 33(1): 259-265.
7. Heiligers, J., Parker, J. S., and Macdonald, M., "Novel solar-sail mission concepts for high-latitude Earth and lunar observation," *Journal of Guidance, Control, and Dynamics*, 2017;1-19.
8. Walmsley, M., Heiligers, J., Ceriotti, M., and McInnes, C., "Optimal trajectories for planetary pole-sitter missionsj," *Journal of Guidance, Control, and Dynamics*, 2016; 39(10): 2461-2468.
9. Anderson, P., Macdonald, M., and Yen, C. W., "Novel orbits of Mercury, Venus and Mars enabled using low-thrust propulsion," *Acta Astronautica*, 2014; 94:635-645.
10. LeCompte, M., Meyer, T. R., Horsewood, J., and Durda, D. D., "Early, short-duration, near-Earth-asteroid rendezvous missions," *Journal of Spacecraft and Rockets*, 2012; 49(4): 731-741.
11. Biggs, J. D., C. R. McInnes and T. Waters. "Control of solar sail periodic orbits in the elliptic three-body problem." *Journal of Guidance, Control, and Dynamics*, 2009; 32(1): 318-320.
12. Heiligers, J., D. Guerrant and D. Lawrence. "Exploring the heliogyro's orbital control capabilities for solar sail halo orbits." *Journal of Guidance, Control, and Dynamics*, 2017: 40(10): 2569-2586.

13. Heiligers, J., Ceriotti, M, McInnes C. R., Biggs, J D. "Design of optimal earth pole-sitter transfers using low-thrust propulsion." *Acta Astronautica*, 2012; 79 (79) :253-268.
14. Baig, S., and McInnes, C. R., "Light-levitated geostationary cylindrical orbits are feasible," *Journal of Guidance, Control, and Dynamics*, 2010; 33(3): 782-793.
15. McInnes, C. R., "Solar sailing: technology, dynamics and mission applications," *Springer-Praxis Books in Astronautical Engineering*, *Springer Verlag*, 1999: 1-40.
16. Hirai, T., Yano, H., Fujii, M., Hasegawa, S., Moriyama, N., Okamoto, C., and Tanaka, Makoto., "Data screening and reduction in interplanetary dust measurement by IKAROS-ALADDIN," *Advances in Space Research*, 2017; 59(6): 1450-1459.
17. Newton, K., "NASA's first solar sail NanoSail-D deploys in low Earth orbit" [online], *NASA Marshall Space Flight Center*, Huntsville, 2011, http://www.nasa.gov/centers/marshall/news/news/releases/2011/11-010.html
18. Johnson, L., Young, R., Barnes, N., Friedman, L., Lappas, V., and McInnes, C., "Solar sails: technology and demonstration status," *International Journal of Aeronautical and Space Sciences*, 2012;13(4): 421-427.
19. Leslie, M. N., Les, J., Dennon, C., Julie, C. R., Andreas, F., and Laura, J., "Near-Earth asteroid Scout," *AIAA SPACE 2014 Conference and Exposition, San Diego*, CA, 2014.
20. McInnes, C. R., and Simmons, J. F. L., "Solar sail halo orbits. Part I - Heliocentric case," *Journal of Spacecraft and Rockets*, 1992. 29(4): 466-471.
21. McInnes, C. R., and Simmons, J. F. L., "Solar sail halo orbit. Part II - Geocentric case," *Journal of Spacecraft and Rockets*, 1992. 29(4): p. 472-479.
22. Macdonald, M., and McInnes, C. R., "Solar sail science mission applications and advancement," *Advances in Space Research*, 2011. 48(11): 1702-1716.
23. Heiligers, J., and McInnes, C. R., "New Families of sun-centered non-Keplerian orbits over cylinders and spheres," *Celestial Mechanics and Dynamical Astronomy*, 2014. 120(2): 163-194.
24. "Mission to asteroid 9969 Braille, comet Borrelly Deep Space 1" [online], *Jet Propulsion Laboratory*, 1998, https://www.jpl.nasa.gov/missions/deep-space-1-ds1/ [retrieved 12 May. 2010].
25. "GOCE "[online], *ESA*, 2009,http://www.esa.int/Our_Activities/Observing_the_Earth/GOCE/Satellite [retrieved 20 Feb. 2015].
26. "SMART-1" [online], *ESA*, 2006, http://sci.esa.int/smart-1/ [retrieved 15 Oct. 2016].
27. Gong, S. P., Li, J. F., and Jiang, F. H., "Interplanetary trajectory design for a hybrid propulsion system," *Aerospace*

*Science and Technology*, 2015; 45:104-113.

28. Mengali, G., and Quarta, A. A., "Trajectory design with hybrid low thrust propulsion system," *Journal of Guidance*, *Control*, *and Dynamics*, 2007; 30(2): 419-426.
29. Mengali, G., and Quarta, A. A., "Tradeoff performance of hybrid low thrust propulsion system," *Journal of Spacecraft and Rockets*, 2007; 44(6): 1263-1270.
30. Simo, J., and McInnes, C. R., "Displaced periodic orbits with low thrust propulsion," *19th AAS/AIAA Space Flight Mechanics Meeting*, Savannah, GA, American Astronomical, Washington D C, 2009.
31. Brophy, J., "Advanced ion propulsion systems for affordable deep space missions,". *Acta Astronautica*, 2003; 52(2): 309-316.
32. Reissner, N. Buldrini, B. Seifert, F. Plesescu, C. Scharlemann, and J. G. del Amo, "mN-FEEP thruster module design and preliminary performance testing," *33rd International Electric Propulsion Conference*, Washington, 2013.
33. Becerra, V. M., "Solving complex optimal control problems at no cost with PSOPT," *IEEE International Symposium on Computer-Aided Control System Design* (*CACSD*), Piscataway, 2010: 1391-1396.
34. Evans, B. G., "Satellite communication systems," *International Journal of Satellite Communications & Networking*, 2010, 6(3):361-361.
35. "Long-Term Sustainability of Outer Space Activities, Preliminary Reflections," *United Nations, Committee on the Peaceful Uses of Outer Space, Scientific and Technical Subcommittee*, 47th Session, Rept. A/AC.105/C.1/2010/CRP.3, Feb. 2010.
36. Ceriotti, M., and McInnes, C. R., "Systems design of a hybrid sail pole-sitter," *Advances in Space Research*, 2011; 48(11): 1754-1762.
37. Gershman, R., and Seybold, C., "Propulsion trades for space science missions," *Acta Astronautica*, 1999; 45:541-548.
38. Kitamura, S., Ohkawa, Y,. Hayakawa, Y., Yoshida, H., and Miyazaki, K., "Overview and research status of the JAXA 150-mN ion engine," *Acta Astronautica*, 2007; 61: 360-366.
39. Dachwald, B., "Optimal solar sail trajectories for missions to the outer solar system." *Journal of Guidance*, *Control*, *and Dynamics*, 2005; 28(6):1187-1193.

**Yuan LIU** is a lecture at college of automation, Harbin Engineering University, Harbin, China. He received the Ph.D. degree from the Harbin Institute of Technology in 2010. Her current research interests are orbit dynamic, planning and control.

E-mail: ericliuprc@hotmail.com

**Matteo CERIOTTI** is a lecturer in Space Systems Engineering, within the School of Engineering, division of Systems Power & Energy, University of Glasgow, United Kingdom. He received the Ph.D. degree from the same university. His current research interests are in space mission analysis and trajectory design, orbital dynamics, trajectory optimization, and spacecraft autonomy.

E-mail: Matteo.Ceriotti@glasgow.ac.uk

**Jeannette HEILIGERS** is a Marie Skłodowska-Curie Research Fellow at the Astrodynamics & Space Missions Section, Faculty of Aerospace Engineering, Delft University of Technology, the Netherlands. She received her Ph.D. degree from the University of Strathclyde, United Kingdom. Her current research interests are in advanced space mission concepts, space mission analysis & design, astrodynamics, orbital dynamics, trajectory optimisation, low-thrust propulsion, and solar sailing.

E-mail: m.j.heiligers@tudelft.nl